Earth and Planetary Science Letters 329-330 (2012) 84–96

Contents lists available at SciVerse ScienceDirect

Earth and Planetary Science Letters

journal homepage: www.elsevier.com/locate/epsl

Asthenosphere–lithosphere interaction triggered by a slab window during ridge subduction: Trace element and Sr–Nd–Hf–Os isotopic evidence from Late Carboniferous tholeiites in the western Junggar area (NW China)

Gong-Jian Tang [a,b], Derek A. Wyman [c], Qiang Wang [a,*], Jie Li [a], Zheng-Xiang Li [d], Zhen-Hua Zhao [a], Wei-Dong Sun [a]

[a] State Key Laboratory of Isotope Geochemistry, Guangzhou Institute of Geochemistry, Chinese Academy of Sciences, Guangzhou 510640, China
[b] Graduate University of Chinese Academy of Sciences, Beijing 100049, PR China
[c] School of Geosciences, Division of Geology and Geophysics, The University of Sydney, NSW 2006, Australia
[d] ARC Centre of Excellence for Core to Crust Fluid Systems (CCFS) and The Institute for Geoscience Research (TIGeR), Department of Applied Geology, Curtin University, GPO Box U1987, Perth, WA 6845, Australia

ARTICLE INFO

Article history:
Received 8 April 2011
Received in revised form 13 February 2012
Accepted 14 February 2012
Available online 22 March 2012

Editor: R.W. Carlson

Keywords:
tholeiites
slab window
ridge subduction
asthenosphere
Central Asian Orogenic Belt

ABSTRACT

Tholeiites occur in a variety of geological settings, e.g., mid-ocean ridge, back-arc basin, ocean island, island arc and intra-continent, and their geochemical and isotopic characteristics vary according to the corresponding geodynamic environments. Here we investigated the Hatu tholeiitic basalts and basaltic andesites of the western Junggar region, Central Asian Orogenic Belt (CAOB). LA-ICPMS zircon U–Pb analyses indicate that the Hatu tholeiites were generated in the Late Carboniferous (~315 Ma). All the studied rock samples are characterized by flat rare earth elements pattern on chondrite-normalized plot, and negligible Nb, Ta and Ti anomalies on mid-ocean-ridge basalt normalized plots. They are also characterized by moderate positive $\varepsilon_{Nd}(t)$ (+5.25 to +5.94), $\varepsilon_{Hf}(t)$ (+13.24 to +14.89), highly radiogenic Os isotope compositions ($^{187}Os/^{188}Os_{315Ma}$ = 0.1338–0.3547), and relatively low ($^{87}Sr/^{86}Sr)_i$ ratios (0.7044 to 0.7048). Taking into account their geological characteristics, the occurrence of nearby ophiolites and the types of contemporaneous magmatic rocks found in the western Junggar region, we propose that the Hatu basalts were generated by slab window-related processes following a spreading ridge subduction beneath the Keramay intra-oceanic island arc. During this process, deep and enriched asthenospheric mantle rose to the edge of the subducted oceanic lithosphere, its melts infiltrating the subducted oceanic lithosphere and reacting with peridotites. Therefore, the Hatu tholeiites are interpreted as a result of melting of a mixed mantle source consisting of subducted depleted oceanic lithosphere and a deep, enriched upwelling asthenospheric mantle. Incongruent dynamic melting modeling of trace element compositions indicates that the Hatu basalts could have been derived from large degrees of melting (~10%) of such a mixed mantle source. This newly recognized mechanism is a natural consequence of the diversity of contemporaneous potential mantle sources available in slab window settings.

1. Introduction

Tholeiitic magmas are voluminous and occur in a wide variety of geological settings, and are derived from numerous geodynamically distinct sources (e.g., depleted MORB mantle, enriched plume-related mantle, subcontinental lithospheric mantle, and subduction component-enriched mantle: Kerr et al., 2002; Pearce et al., 2005; Sun and McDonough, 1989; Xu et al., 2005). Tholeiitic magmas associated with slab windows, resulting from oceanic spreading ridge subduction, are derived from sources that encompass diverse characteristics. Sub- and supra-slab mantle reservoirs and the down-going slab itself may all act as sources for basaltic magmas that range from depleted and MORB-like (e.g., southern Alaska) to enriched OIB (oceanic island basalt) in composition (e.g., southern Patagonia) (Cole and Stewart, 2009; Gorring et al., 2003; Hole et al., 1991). These "slab window basalts" provide an opportunity to explore the enrichment processes and compositionally heterogeneous mantle sources associated with a geodynamic setting that is now considered a common and important consequence of plate subduction (e.g., Cole and Stewart, 2009; Windley et al., 2007).

The Central Asian Orogenic Belt (CAOB), also known as the Altaid Tectonic Collage, is one of the largest orogens in the world and comprises island arcs, seamounts, accretionary wedges, oceanic plateaux and, possibly, microcontinents accreted during the closure of the Paleo-Asian Ocean (Jahn et al., 2000; Kröner et al., 2007; Sengör et al., 1993; Xiao et al., 2008). It extends from the Urals in the west,

* Corresponding author.
E-mail address: wqiang@gig.ac.cn (Q. Wang).

0012-821X/$ – see front matter © 2012 Elsevier B.V. All rights reserved.
doi:10.1016/j.epsl.2012.02.009

through Kazakhstan, northern China, and Mongolia to the eastern Russian coast (Fig. 1a). The CAOB represents a site of major crustal growth in the Phanerozoic and at least half of its growth was due to the addition of mantle-derived juvenile material (Jahn et al., 2000; Sengör et al., 1993). However, the mechanisms of crustal growth for the CAOB are not well understood. Sengör et al. proposed that the CAOB grew by the addition of arc complexes from the early Cambrian (~540 Ma) to the Permian (~260 Ma) (Sengör and Natal'in, 1996; Sengör et al., 1993). In contrast, many studies have argued that Phanerozoic CAOB granitoids, which are characterized by positive ε_{Nd} values, were generated by extensive underplating of mantle-derived basaltic magmas in a post-orogenic or intra-plate extensional setting (Jahn et al., 2000; Wu et al., 2002). More recently, Windley et al. (2007) suggested that the CAOB contains many key features that may be related to Paleozoic ridge subduction, and a number of local case studies within the CAOB support the ridge subduction model (Geng et al., 2009; Jian et al., 2008; Sun et al., 2009; Tang et al., 2010, 2012a,b). In addition, an Early Permian (280–270 Ma) mantle plume model has also been proposed for tectonic evolution in Tarim and the CAOB (e.g., Zhang et al., 2010; Zhou et al., 2004, 2009).

The western Junggar region in the southwestern CAOB is a key area for deciphering the tectonic evolution and crustal growth within the orogenic belt. The region contains voluminous Late Paleozoic granitoids and volcanic rocks with positive $\varepsilon_{Nd}(t)$ (Chen and Arakawa, 2005; Geng et al., 2009; Tang et al., 2010, 2012a,b). However, the petrogenesis and tectonic environments of the Late Carboniferous to Early Permian (320–290 Ma) magmatism are still controversial for the region, with two major competing viewpoints

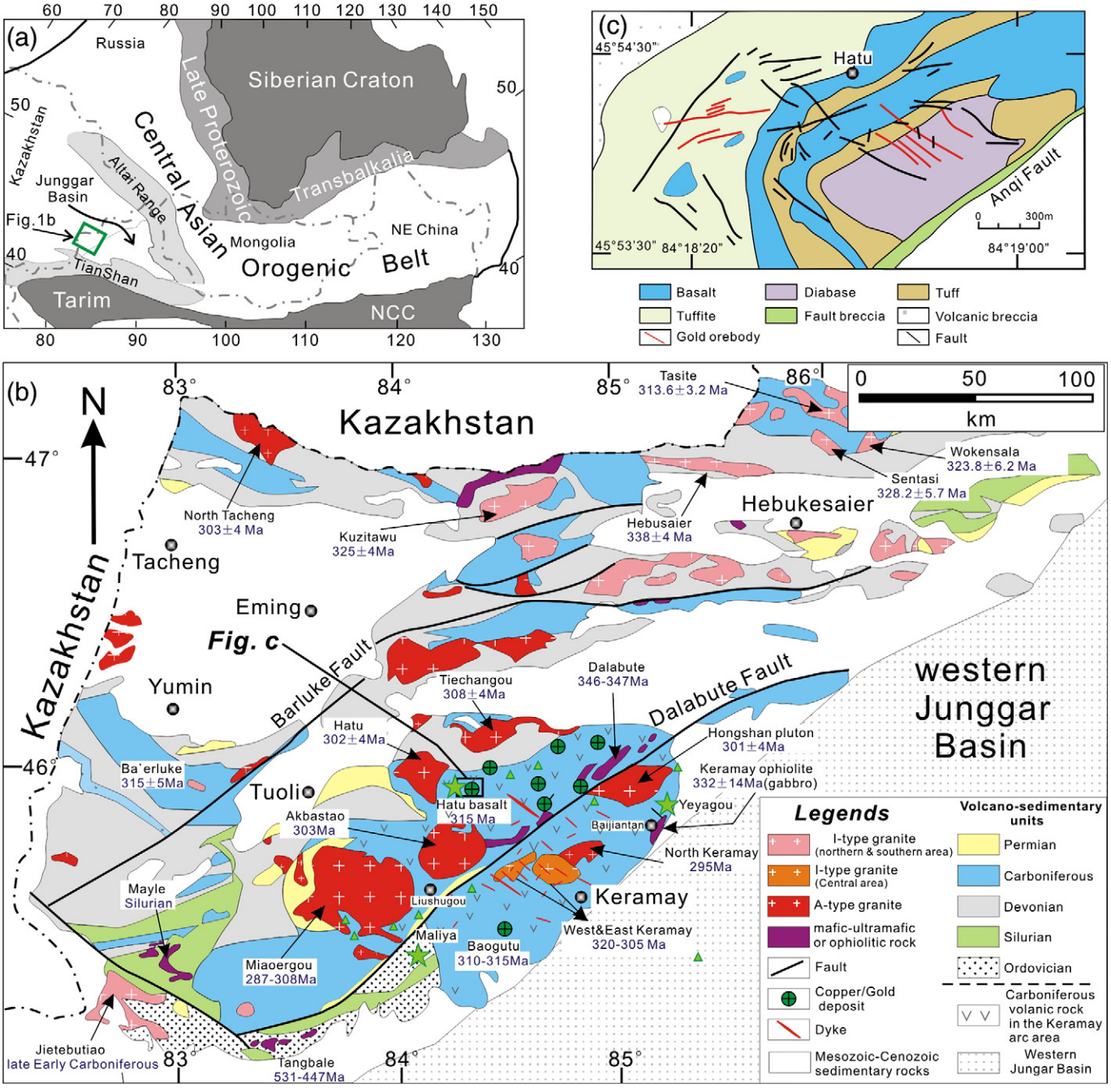

Fig. 1. (a) Simplified tectonic divisions of the CAOB (after Jahn et al., 2000). (b) Geological map of the western Junggar region (modified after XBGMR (Xinjiang Bureau of Geology and Mineral Resources), 1993). Jade-green triangle: site of Early Carboniferous basalt; Jade-green star: Late Carboniferous basalt. (c) Simplified geological map of the Hatu deposit (after Shen et al., 1993). NCC — North China Craton.

being proposed, i.e., post-collisional (Chen and Arakawa, 2005; Han et al., 2006; Su et al., 2006) versus an island arc environment related to intra-oceanic subduction or ridge subduction (Geng et al., 2009; Tang et al., 2010, 2012a,b; Xiao et al., 2008; Yin et al., 2010; Zhang et al., 2006). Previous studies mainly focused on the intermediate-felsic rocks (e.g., adakites and A-type granites) and the petrogenesis of basalts in the western Junggar is still poorly constrained. Therefore, in this paper we focus on the Hatu basalts from this region. Based on new geochronology, major and trace element and Sr–Nd–Hf–Os isotope data, we show that the Late Carboniferous Hatu basalts are tholeiitic, geochemically oceanic plateau-like basalts, and were probably generated in a distinctive island arc setting related to a slab window induced by ridge subduction. They were most plausibly derived from a mixed mantle source region composed of subducted oceanic depleted lithosphere and a deep, enriched upwelling asthenospheric mantle, with a small contribution from an enriched, subducted sedimentary component. Our study, therefore, not only proposes a new mechanism for the petrogenesis of tholeiitic magmas, but also provides important evidence for genetic links between the Late Carboniferous magmatism and ridge subduction in the western Junggar region.

2. Geological background and rock characteristics

The western Junggar region is surrounded by the Altai Orogen to the north, the Tianshan Orogen to the south, the Kazakhstan Plate to the west, and the Junggar Basin to the east (Fig. 1b). Post-Cambrian (Ordovician–Quaternary) sedimentary rocks, particularly Devonian and Carboniferous volcanic-sedimentary rocks, are abundant in the region (Fig. 1b). The Carboniferous strata, from the oldest to the youngest, are composed of the Xibeikulasi, Baogutu and Tailegula formations (An and Zhu, 2009) (Supplemental file 1). Carboniferous to early Permian (320–290 Ma) granitoid intrusions are widely distributed in the region (Chen and Arakawa, 2005; Geng et al., 2009; Han et al., 2006; Tang et al., 2010, 2012a,b). Many ophiolitic mafic–ultramafic rocks also occur in the western Junggar region, and their ages range from the Cambrian to the Late Carboniferous (Fig. 1b) (Beijing SHRIMP Unit, 2005; Xu et al., 2006a).

Late Carboniferous basalts occur mainly in the Hatu, Yeyagou and Maliya areas in the central part of the western Junggar region (Fig. 1b). The Hatu basalts are distributed along a northeast trend that is >100 km long and ~10 km in width (Fig. 1c). The Hatu basalts occur in the lower unit of the Tailegula Formation, which consists of basalt, dolerite, tuff, siltstone and sandstone, whereas the upper unit consists of tuff sandstone, siltstone and mudstone. Isotopic ages, fossils (coral: *Kinkaidia* and *Fasciculophyllum;* brachiopoda: *Syriugothyris* and *Rotaia*) and the interbedded relationships of the Carboniferous volcanic-sedimentary strata constrain the age of the Tailegula Formation to the Late Carboniferous. Tailegula Formation basalts from the Qiqiu gold deposit yielded ages of 296.60 ± 0.95 Ma and 311.91 ± 0.45 Ma by ^{40}Ar–^{30}Ar dating (Hu et al., 1997). Siliceous rocks from the Tailegula Formation in the Hatu gold deposit gave a whole rock Rb–Sr age of 316 ± 21 Ma (Li et al., 2000). Zircon SHRIMP dating of felsic tuffs from the Tailegula Formation at the Baobei gold deposit gave a concordant U–Pb age of 328.1 ± 1.8 Ma (Wang and Zhu, 2007). The Tailegula Formation is younger than the Baogutu Formation based on the field geological relationship, and the latter formed at 345–326 Ma, based on zircon LA-ICPMS dating (An and Zhu, 2009).

Numerous Cu–Au deposits occur in the central area of the western Junggar region (Fig. 1b). The mineralization ages of these deposits are nearly identical to zircon U–Pb ages of the western Junggar Hatu basalts and Baogutu adakites (~315 Ma: Tang et al., 2010; this study): (1) molybdenite from the Baogutu deposit gives Re–Os ages of 310 ± 4 Ma and 312.4 ± 1.8 Ma, respectively (Shen et al., 2012; Song et al., 2007); and (2) a gold-bearing quartz vein in the Hatu gold deposit yielded a $^{40}Ar/^{39}Ar$ age of 308.6 ± 4.2 Ma (Shen et al., 1993).

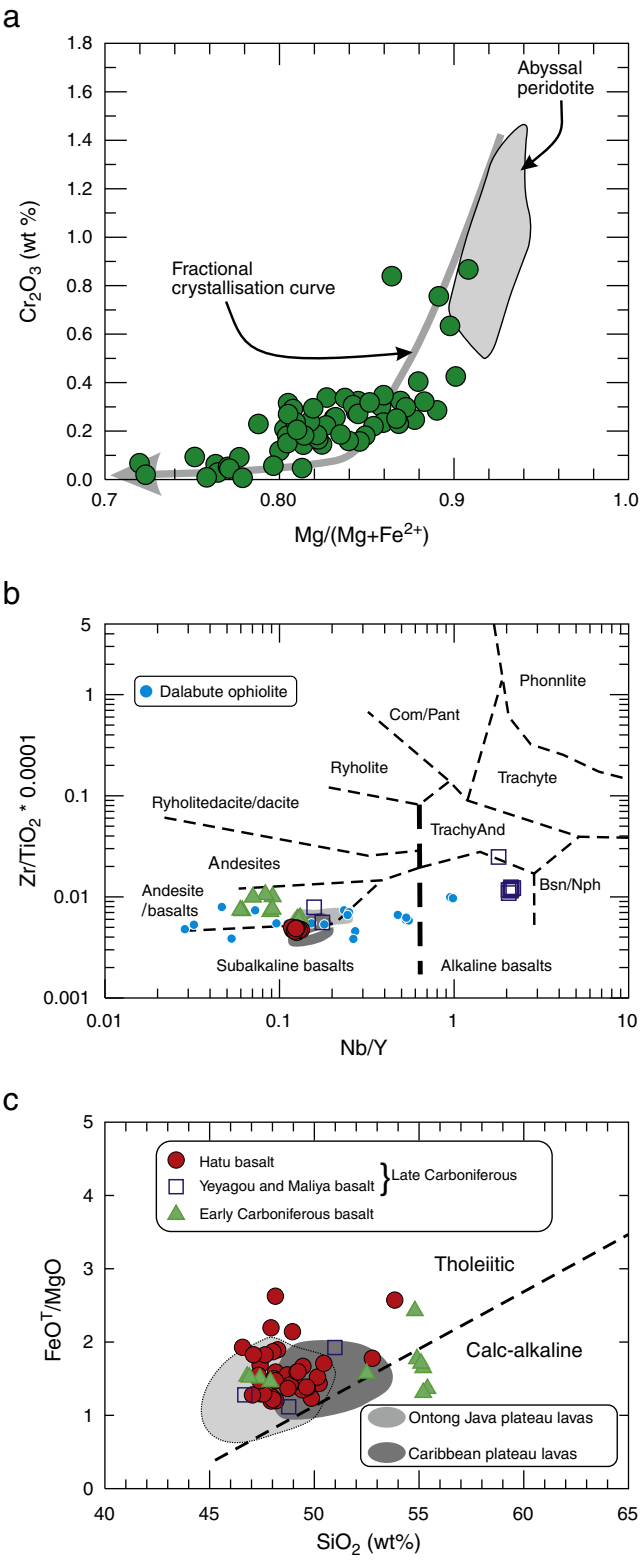

Fig. 2. (a) Mg/(Mg + Fe^{2+}) vs. Cr_2O_3 content of clinopyroxene from Hatu basalts in the western Junggar region, southwestern part of the CAOB. Abyssal peridotite field taken from Johnson et al. (1990), fractional crystallization curve from Constantin (1999). (b) $Zr/TiO_2 \times 0.0001$ versus Nb/Y diagram distinguishing subalkaline and alkaline basalts (Winchester and Floyd, 1977). (c) FeO^T/MgO versus SiO_2 diagram distinguishing tholeiitic and calc-alkaline series (Miyashiro, 1974). Data for Late Carboniferous basalts in the Yeyagou and Maliya areas of western Junggar region are from Zhang (2009). Data for Early Carboniferous basalts in western Junggar region are from Geng et al. (2011). Data for basalts of the Dalabute ophiolites are from Liu et al. (2009), and references therein. Data for Ontong Java and Caribbean oceanic plateau lavas are from Fitton and Godard (2004) and Hastie et al. (2008).

The Hatu basalts have porphyritic texture with phenocrysts of clinopyroxene, plagioclase and minor olivine. The groundmass is composed of fine-grained clinopyroxene, plagioclase, orthopyroxene, olivine, chlorite, magnetite, plus glass and cryptocrystalline materials. The clinopyroxene phenocrysts are euhedral–subhedral and up to 1.0 mm in diameter.

3. Results

Analytical methods, zircon U–Pb data and diagrams, and clinopyroxene compositions data for the Hatu basalts are listed in Supplemental files 2–5, respectively. We selected least altered samples with little or no mineralization for geochemical and isotopic analyses.

3.1. Geochronology

In order to determinate the absolute age of the basalts from the western Junggar region, a sample was selected for zircon U–Pb analysis (06XJ163) (Supplemental files 3 and 4a). For zircon U–Pb dating, thirty-four analyses of zircons from the Hatu basalt sample 06XJ163 give a weighted mean $^{206}Pb/^{238}U$ age of 315 ± 4 Ma (2σ) (mean square weighted deviation (MSWD) = 0.43). Spot 04 gives the oldest $^{206}Pb/^{238}U$ age of ~400 Ma, interpreted as the age of captured zircons from volcanic country rocks. Three other analyses give $^{206}Pb/^{238}U$ ages ranging from 271 Ma to 293 Ma and the data depart from the concordia line, which suggests that these zircons have undergone Pb loss (Supplemental file 4a).

3.2. Mineral composition

All clinopyroxenes crystals in the Hatu basalts from the western Junggar region are augite, with $Mg^{\#}$ ($100 \times$[atomic MgO/(MgO + FeO)]) values in the range of 72–91. Their Al_2O_3, Cr_2O_3 and TiO_2 contents range from 1.27 to 4.50 wt.%, 0 to 0.87 wt.% and 0.15 to 0.97 wt.%, respectively (Supplemental file 5). All clinopyroxene analyses follow the main oceanic tholeiitic fractional crystallization trend of Constantin (1999) (Fig. 2a).

Table 1
Major (wt.%) and trace (ppm) element compositions for the Hatu basalts.

Sample	06XJ160-1	06XJ160-2	06XJ161-1	06XJ161-2	06XJ162	06XJ163-1	06XJ163-2	06XJ163-3	06XJ164-1	06XJ164-2	06XJ165
Longitude	84°19′03″N		84°18′52″N		84°18′40″	84°18′41″N			84°18′29″N		84°18′29″
Latitude	45°54′27″E		45°54′26″E		45°54′24″	45°54′24″E			45°54′07″E		45°54′05″
SiO_2	48.14	52.77	49.18	49.22	47.32	48.03	47.65	47.10	48.74	49.63	50.45
Al_2O_3	13.99	13.77	13.87	13.29	13.96	14.53	14.68	14.61	14.06	13.81	13.85
TiO_2	1.22	1.45	1.22	1.25	1.00	1.26	1.28	1.27	1.09	1.11	1.20
MnO	0.17	0.17	0.19	0.21	0.18	0.20	0.20	0.21	0.17	0.17	0.20
MgO	8.27	7.19	7.68	7.82	7.61	6.75	7.10	7.18	8.39	8.05	6.91
FeO	12.18	12.78	12.22	12.47	11.76	12.61	12.96	13.11	11.47	11.15	11.81
CaO	4.84	4.84	7.91	7.98	10.89	8.39	7.73	8.38	5.27	5.35	7.76
Na_2O	2.83	4.00	3.56	3.55	2.04	3.32	3.43	3.27	2.27	2.39	3.84
K_2O	0.48	0.38	0.27	0.19	0.12	0.15	0.12	0.13	0.50	0.47	0.28
P_2O_5	0.08	0.09	0.07	0.07	0.06	0.08	0.08	0.08	0.07	0.07	0.08
LOI	6.51	0.70	2.08	2.21	3.53	3.00	3.09	2.90	6.89	6.67	1.93
Total	100.07	99.56	99.62	99.65	99.78	99.72	99.75	99.71	100.19	100.11	99.63
$Mg^{\#}$	54.76	50.10	52.83	52.76	53.57	48.82	49.41	49.41	56.60	56.26	51.03
Sc	51.4	53.8	52.4	52.2	49.2	50.6	50.4	53.6	49.8	48.5	48.4
V	368	389	402	393	363	406	401	421	367	360	375
Cr	269	122	144	155	279	112	110	115	300	287	95.3
Co	54.9	62.7	56.0	57.8	55.1	55.3	76.7	58.1	51.1	51.1	50.1
Ni	106	86.1	87.9	93.7	109	79.1	81.6	85.5	109	107	75.6
Ga	15.8	13.1	16.1	14.6	15.0	16.7	15.5	16.9	12.7	12.1	15.8
Ge	1.80	1.82	1.69	1.71	1.89	2.10	1.83	1.94	1.63	1.53	1.73
Rb	14.2	10.2	5.61	3.44	1.71	2.27	1.70	2.02	11.0	10.0	4.59
Sr	77.0	84.8	189	170	63.3	87.9	95.9	107	152	165	127
Y	23.0	25.5	22.0	21.9	20.6	23.7	23.3	24.2	20.4	20.0	22.8
Zr	57.5	64.6	58.3	58.9	49.8	60.6	60.2	62.1	51.4	51.0	58.3
Nb	2.73	3.19	2.82	2.91	2.42	2.97	3.01	3.03	2.49	2.44	2.83
Cs	7.85	4.65	2.50	1.81	0.530	1.85	2.40	2.56	5.34	4.95	2.56
Ba	65.5	58.9	45.1	29.0	20.5	74.5	74.5	81.4	105	98.4	116
La	3.37	3.80	2.94	2.96	2.85	3.38	3.17	3.41	2.76	2.73	3.20
Ce	9.18	9.82	7.95	8.13	7.82	8.92	8.89	9.40	7.64	7.47	8.70
Pr	1.50	1.61	1.29	1.36	1.29	1.47	1.47	1.50	1.26	1.24	1.44
Nd	7.66	8.27	6.75	6.95	6.49	7.47	7.65	7.89	6.45	6.41	7.43
Sm	2.43	2.69	2.20	2.31	2.14	2.42	2.50	2.50	2.12	2.14	2.43
Eu	0.934	1.08	0.956	0.972	0.850	0.947	0.959	0.973	0.837	0.837	0.980
Gd	3.23	3.59	3.00	3.11	2.96	3.22	3.37	3.38	2.78	2.77	3.23
Tb	0.628	0.721	0.587	0.612	0.577	0.635	0.662	0.662	0.540	0.548	0.631
Dy	4.06	4.77	3.93	4.10	3.80	4.28	4.30	4.40	3.56	3.53	4.19
Ho	0.869	1.05	0.861	0.895	0.840	0.954	0.961	0.976	0.794	0.770	0.915
Er	2.51	2.97	2.50	2.56	2.31	2.77	2.69	2.75	2.24	2.26	2.67
Tm	0.366	0.432	0.359	0.381	0.342	0.406	0.395	0.416	0.345	0.338	0.387
Yb	2.40	2.90	2.41	2.61	2.28	2.65	2.59	2.71	2.20	2.20	2.54
Lu	0.369	0.431	0.380	0.399	0.358	0.405	0.403	0.413	0.343	0.345	0.389
Hf	1.79	2.11	1.84	1.96	1.67	1.93	1.97	2.01	1.62	1.62	1.84
Ta	0.197	0.247	0.212	0.223	0.200	0.221	0.235	0.227	0.187	0.182	0.208
Pb	0.802	0.520	0.173	0.476	0.074	0.245	0.281	0.203	0.268	0.236	0.165
Th	0.298	0.356	0.305	0.312	0.293	0.339	0.335	0.340	0.285	0.285	0.315
U	0.067	0.078	0.069	0.070	0.066	0.072	0.073	0.076	0.065	0.061	0.068

$Mg^{\#} = 100 \times$[atomic MgO/(MgO + FeO)]. LOI weight loss on ignition to 900 °C.

3.3. Major and trace elements geochemistry

The Hatu basalts display a wide range of SiO_2 contents (46 to 54 wt.%), but the majority of the samples fall between 47 and 50 wt.% (Table 1). They also have a wide range of $Mg^{\#}$ ($100\times$[atomic MgO/(MgO + FeO)]), ranging from 40 to 60, indicating that they have experienced minor to moderate differentiation. On the Zr/TiO_2–Nb/Y diagram of Winchester and Floyd (1977), all the Hatu basalt samples plot in the subalkaline field as a result of Nb/Y ratios between 0.12 and 0.13 (Fig. 2b). The basalts also define a typical tholeiite compositional trend on the SiO_2–FeO^T/MgO diagram (Fig. 2c). The Hatu basalts have TiO_2 content ranging from 0.85 to 2.2 wt.%. They are similar to basalts closely associated with slab windows as a result of ridge subduction (i.e., the slab window basalts of Cole and Stewart (2009)).

The Hatu basalts have very uniform chondrite-normalized rare earth element (REE) patterns, with no distinctive fractionation characteristics and negligible Eu anomalies (Supplemental file 6a). The Hatu basalts have $(La/Sm)_N$ ratios ranging from 0.8 to 0.9 that are higher than N-MORB (0.6), but $(Gd/Yb)_N$ ratios that are nearly identical to N-MORB (0.99) (Sun and McDonough, 1989). Trace-element distribution patterns of most Hatu basalt samples are characterized by a lack of Nb, Ta and Ti anomalies on N-MORB-normalized diagrams, indicating no back-arc affinity (Fig. 3). Compared to typical N-MORB, the Hatu basalts have higher Th, U, Nb, Ta and light REE (LREE) concentrations and lower heavy REE (HREE) concentrations (Fig. 3a). The major and trace element abundances show that the Hatu basalts have compositions similar to lavas from the Ontong Java or the Caribbean plateau and transitional from the composition of average MORB to OIB (Figs. 2 and 3; Supplemental file 6b).

3.4. Sr–Nd–Hf–Os isotopes geochemistry

Initial isotopic ratios of the Hatu basalts were calculated based on a formation age of 315 Ma (Table 2) (see a detailed discussion in the following section). The Hatu basalts have $(^{87}Sr/^{86}Sr)_i$ values ranging from 0.7044 to 0.7048 (Table 2), except for one sample (06XJ163-2) that has an $(^{87}Sr/^{86}Sr)_i$ value of 0.7051. All samples have quite uniform $\varepsilon_{Nd}(t)$ (+5.3 to +6.0) (Fig. 4a), initial $^{176}Hf/^{177}Hf$ (0.282950–0.282997) and $\varepsilon_{Hf}(t)$ (+13.2 to +14.8) values (Table 2). All samples plot above the mantle array [$\varepsilon_{Hf}(t) = 1.59\varepsilon_{Nd}(t) + 1.28$] of Chauvel et al. (2008) on the $\varepsilon_{Hf}(t)$ versus $\varepsilon_{Nd}(t)$ diagram (Supplemental file 6c).

Rhenium and osmium concentrations in the Hatu basalts range from 0.14 to 1.80 ng/g and 35 to 326 pg/g, respectively (Table 2). Osmium isotope compositions display a considerable range, from 0.1338 to 0.3547 ($^{187}Os/^{188}Os_{315Ma}$), coupled with widely ranging $^{187}Re/^{188}Os$ ratios (5.2 to 178). Initial $^{187}Os/^{188}Os$ ratios are inversely correlated with MgO and Os concentrations (Fig. 4b, c). The negative covariation between Os abundance and initial $^{187}Os/^{188}Os$ is consistent with a mixing process between the 'true' initial isotope composition and a radiogenic contaminant. Os is strongly compatible during mantle melting (Shirey and Walker, 1998) and is strongly concentrated in the mantle but extremely depleted in the crust. Given the relatively high Os concentrations of the Hatu basalts, seawater alteration or crustal contamination effects are too small to significantly modify the Os isotope compositions in most of the samples. Thus, the high Os (>80 pg/g) Hatu samples retain their Os isotopic characteristics from a mantle source or sources, although three low Os samples (<60 pg/g) with high initial $^{187}Os/^{188}Os$ ratios may have been slightly modified by shallow level contamination.

4. Discussion

4.1. Epochs of magmatic activities in the western Junggar

The well-defined zircon U–Pb age of 315 ± 4 Ma obtained in this study for the Hatu basalts (Supplemental file 4a) establishes the

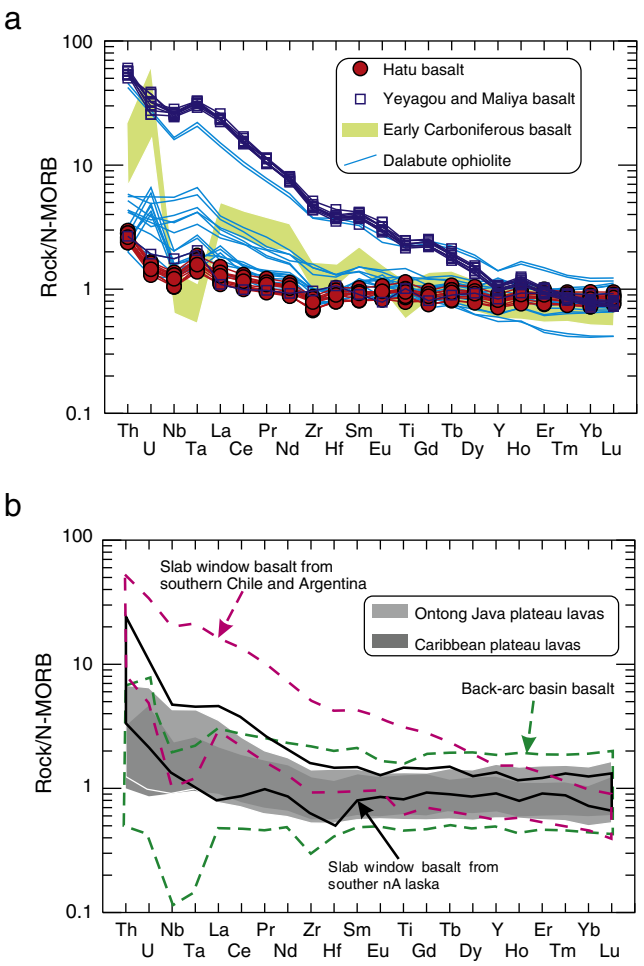

Fig. 3. N-MORB normalized trace element diagrams for the Hatu basalt samples from the western Junggar compared with other slab window basalts and BABB (back-arc basin basalts). N-MORB normalized values are from Sun and McDonough (1989). Slab window basalts from southern Alaska are from Cole et al. (2006), slab window basalts from southern Chile and Argentina are from Gorring et al. (2003) and D'Orazio et al. (2001). Back-arc-basin basalts are from Fretzdorff et al. (2006), Pearce et al. (2005) and Shinjo et al. (1999). Other data sources are the same as for Fig. 2.

Late Carboniferous eruption age for basalts in the western Junggar region. The Carboniferous–Early Permian time was a critical period in the evolution of the western Junggar district that was punctuated by two major episodes of magmatic activity (~350–330 Ma and 320–290 Ma; Supplemental file 4b). Magmatic rocks of the earlier episode are mainly of the island-arc type basaltic–andesitic–felsic suite, which is scattered throughout the entire western Junggar region (Geng et al., 2011; Tang et al., 2010, 2012a,b; Wang and Zhu, 2007). Magmatic rocks of the younger event include a suite of penecontemporaneous (~320 to 310 Ma) volcanic and sub-volcanic rocks including adakites, high-Mg diorites, tholeiitic basalts and alkaline basalts (Supplemental file 4b) (Geng et al., 2009; Han et al., 2006; Tang et al., 2010, 2012a,b; Yin et al., 2010) and 310–290 Ma A-type granites (Geng et al., 2009; Han et al., 2006). The Late Carboniferous tholeiitic and alkaline basalts (e.g., those in the Yeyagou (306 Ma) and Maliya (311 Ma) areas) display N-MORB to OIB affinities (Fig. 3; Zhang (2009)).

4.2. Effects of alteration, crustal contamination and fractionation

The Hatu basalts have variably high LOI values (0.70–6.89 wt.%), and the ubiquitous presence of secondary minerals replacing the primary igneous minerals, indicating that they have undergone significant alteration and the abundance of some mobile trace elements could have

Table 2
Sr, Nd, Hf and Os isotopic compositions of the Hatu basalts.

Sample	Rb (ppm)	Sr (ppm)	Sm (ppm)	Nd (ppm)	Lu (ppm)	Hf (ppm)	$^{87}Sr/^{86}Sr$	2σ	$^{143}Nd/^{144}Nd$	2σ	$^{147}Sm/^{144}Nd$	$^{87}Rb/^{86}Sr$	$\varepsilon_{Nd}(t)$	$(^{87}Sr/^{86}Sr)_i$	$^{176}Hf/^{177}Hf$	2σ
06XJ160-1	14.2	77.0	2.43	7.66	0.369	1.79	0.706744	0.000016	0.512927	0.000009	0.1932	0.5186	5.8	0.704715	0.283145	0.000019
06XJ161-2	3.44	170	2.31	6.95	0.399	1.96	0.704701	0.000016	0.512943	0.000010	0.2023	0.0570	5.8	0.704478		
06XJ162	1.71	63.3	2.14	6.49	0.358	1.67	0.705145	0.000020	0.512951	0.000009	0.2010	0.0764	6.0	0.704846	0.283176	0.000021
06XJ163-2	1.70	95.9	2.50	7.65	0.403	1.97	0.705367	0.000017	0.512911	0.000012	0.1988	0.0501	5.3	0.705171	0.283133	0.000015
06XJ164-2	10.0	165	2.14	6.41	0.345	1.62	0.705291	0.000017	0.512951	0.000010	0.2029	0.1708	5.9	0.704623	0.283128	0.000005
06XJ165	4.59	127	2.43	7.43	0.389	1.84	0.705186	0.000017	0.512935	0.000008	0.1994	0.1023	5.7	0.704786	0.283143	0.000004

Sample	$^{176}Lu/^{177}Hf$	$(^{176}Hf/^{177}Hf)_i$	$\varepsilon_{Hf}(t)$	△Hf	Re (ppb)	2σ	Os (ppb)	2σ	$^{187}Os/^{188}Os$	2σ	$^{187}Re/^{188}Os$	2σ	$(^{187}Os/^{188}Os)_i$	$\gamma Os_{(t)}$
06XJ160-1	0.0292	0.282973	13.9	3.1	0.156	0.005	0.1440	0.0007	0.1757	0.0016	5.2	0.2	0.1517	21
06XJ160-1R					0.140	0.003	0.0990	0.0006	0.1682	0.0055	6.8	0.2	0.1368	9
06XJ161-1					1.8	0.3	0.0550	0.0002	1.1749	0.0075	178.6	32. 8	0.3547	183
06XJ161-2					1.647	0.049	0.1520	0.0005	0.4593	0.0027	54.3	1.6	0.2099	67
06XJ162	0.0303	0.282997	14.8	3.7	0.454	0.022	0.3260	0.0021	0.1647	0.0008	6.7	0.3	0.1338	7
06XJ162R					0.342	0.034	0.1010	0.0004	0.2318	0.0016	16.5	1.6	0.1559	24
06XJ163-2	0.0290	0.282962	13.5	3.4	1.5	0.3	0.0530	0.0002	0.9823	0.0041	148.4	27.0	0.3007	140
06XJ164-1					0.854	0.065	0.0880	0.0003	0.4220	0.0016	48.7	3.7	0.1982	58
06XJ164-2	0.0302	0.282950	13.2	2.1	0.636	0.010	0.1770	0.0016	0.2674	0.0033	17.6	0.3	0.1865	49
06XJ165	0.0299	0.282967	13.7	3.0	0.653	0.045	0.0350	0.0001	0.7749	0.0051	96.7	6.7	0.3307	164
06XJ165R					0.576	0.020	0.0610	0.0003	0.4706	0.0046	47.7	1.6	0.2515	101

R-Replicate. $^{87}Sr/^{86}Sr_i = {}^{87}Sr/^{86}Sr - (^{87}Rb/^{86}Sr) \times (e^{\lambda t} - 1)$, $\lambda_{Rb-Sr} = 0.0142\ Ga^{-1}$. $\varepsilon_{Nd}(t) = [(^{143}Nd/^{144}Nd)_{Sample}(t)/(^{143}Nd/^{144}Nd)_{CHUR}(t) - 1] \times 10^4$, $(^{143}Nd/^{144}Nd)_{CHUR}(t) = 0.512638 - 0.1967 \times (\varepsilon^{\lambda t} - 1)$. $\varepsilon_{Hf}(t) = [(^{176}Hf/^{177}Hf)_{Sample}(t)/(^{176}Hf/^{177}Hf)_{CHUR}(t) - 1] \times 10^4$; $\lambda_{Lu-Hf} = 1.93 \times 10^{-11} y^{-1}$. $(^{176}Lu/^{177}Hf)_{CHUR}$, $0 = 0.0332 \pm 2$ $(^{176}Hf/^{177}Hf)_{CHUR}$, $0 = 0.282772 \pm 29$ (Blichert-Toft and Albarède, 1997). $\Delta Hf = \varepsilon_{Hf}(t) - (1.59\varepsilon_{Nd}(t) + 1.28)$ (Chauvel et al., 2008). $^{187}Os/^{188}Os(i) = {}^{187}Os/^{188}O_{Sample} - {}^{187}Re/^{188}Os \times (e^{\lambda t} - 1)$, $\lambda = 1.666 \times 10^{-11} y^{-1}$. $\gamma Os(t) = ((^{187}Os/^{188}Os)(t)/{}^{187}Os/^{188}Os(CHON) - 1) \times 100$, $^{187}Os/^{188}Os(CHON) = 0.1296 - 0.435 \times (e^{\lambda t} - 1)$.

Fig. 4. (a) $\varepsilon_{Nd}(t)$ versus $(^{87}Sr/^{86}Sr)_i$, (b–c) $^{187}Os/^{188}Os_{315Ma}$ plotted as a function of MgO and Os concentrations in Hatu basalts. The fields of recent analogs (Late Miocene to Quaternary) of mafic volcanic rocks that erupted above slab windows from Alaska, Baja California, southern Chile and Argentina, the Antarctic Peninsula, the Kamchatka–Aleutian arc junction, are after Cole and Stewart (2009). Western Junggar granitoids are from Chen and Arakawa (2005); Geng et al. (2009); Baogutu adakites are from Tang et al. (2010). North Xinjiang N-MORB ophiolites are from Xu et al. (2003) and Xu et al. (2006b). OIB array line in panel b is from Chauvel et al. (2008). Other data sources and symbols are the same as for Fig. 2.

been modified (Supplemental file 7). Zirconium is the most immobile element during low-grade alteration and metamorphism, making it the preferred alteration-independent index for assessing the mobility of other trace elements (Polat et al., 2002). For the Hatu basalts, the

alkali metals (such as Rb, K) and alkaline earth metals (such as Ca, Sr, Ba), and Mn show relatively large variations, which do not correlate well with Zr abundances, suggesting that they have undergone variable degrees of mobility during post-magmatic processes (Polat and Hofmann, 2003). Conversely, the high field strength elements (HFSE, such as Nb, Ta, Ti, Zr and Hf), rare earth elements (REE), Y, Th, and U are strongly correlated with Zr, indicating that these elements were essentially immobile during metamorphism and alteration (Polat et al., 2002). Chondrite-normalized REE and primitive-mantle normalized trace-element diagrams generally exhibit smooth and coherent patterns with negligible Ce and Eu anomalies, which also support the limited mobility of the REE (Fig. 3a; Supplemental file 6a) (Polat and Hofmann, 2003). U and Th show a strong linear relationship, whereas Pb and Th do not show a clear relationship, indicating some secondary mobility of Pb (Polat and Hofmann, 2003). Transition metal elements (such as Cr, Co, Sc, V and Ni), MgO, FeO, and Na_2O display coherent trends with Zr (Supplemental file 7), suggesting that these elements were relatively immobile (Polat and Hofmann, 2003). The highly radiogenic initial Os isotope composition (up to 0.3547) in the Hatu samples also suggests that some Re has been lost from the samples as a result of alteration. If we assume that as much as 20% of the Re has been lost for those unexpectedly radiogenic initial Os compositions (0.2 to 0.3547), then the initial $^{187}Os/^{188}Os$ ratios are all reset below 0.25. Rhenium concentrations in MORB range from 0.44 to 2.13 ng/g (Escrig et al., 2005). The Hatu basalts with highly radiogenic initial Os isotope composition (0.3547) also have relatively high Re concentration of 1.8 ng/g. Thus, although those highly radiogenic initial Os isotope compositions are affected to some extent by alteration, they still reflect the isotopic characteristics of the Hatu basalt sources. The following discussion mainly focuses on the abundances and ratios of immobile elements (high field strength elements (HFSE), REE, Y, Th, and U). The rather small ranges of initial $\varepsilon_{Nd}(t)$ and $\varepsilon_{Hf}(t)$ and $(^{87}Sr/^{86}Sr)_i$ values (Table 2) suggest that these are primary values and reflect the isotopic characteristics of the Hatu basalt sources. Considering the mobility of Rb and Sr, only values $(^{87}Sr/^{86}Sr)_i$ for those samples with high Os concentrations (>80 pg/g) were used.

Crustal contamination to the Hatu basalts was minimal as evidenced from the following observations. (1) The presence of positive and homogeneous $\varepsilon_{Nd}(t)$ (+5.26 to +5.96) and $\varepsilon_{Hf}(t)$ (+13.16–+14.81) values and the lack of correlations between $^{147}Sm/^{144}Nd$ and initial $\varepsilon_{Nd}(t)$ values (Table 2), which is a robust evidence against crustal contamination (Vervoort et al., 1999). (2) The negligible Nb and Ta anomalies also suggest that crustal contamination has not played a major role in their evolution (Zhou et al., 2009). The Hatu basalts display LREE depletion ($(La/Sm)_N<1$) associated with positive Nb anomalies where Nb/Th is greater than the primitive mantle value of 8 (Sun and Mcdonough, 1989). The lack of correlation of Nb/Th with $\varepsilon_{Nd}(t)$ (Supplemental file 8) indicates no significant crustal contamination.

In general, mantle-derived primary melts have Ni >400 ppm and Cr >1000 ppm, and $Mg^{\#}=73$–81 (Wilson, 1989). The Hatu basalts show large variations in $Mg^{\#}$ (40–60) and compatible elements such as Cr (66–690 ppm) and Ni (50–242 ppm), indicating that significant fractionation of olivine has occurred. The main phenocrysts observed in the basalts are clinopyroxene and plagioclase, implying that these minerals were the dominant low-pressure fractionation phases. The large variation of $Mg^{\#}$ values (72–91) and Cr_2O_3 contents (0–0.87 wt.%) of the Hatu basalt clinopyroxenes also supports significant fractional crystallization (Fig. 2a).

4.3. Geological and petrological evidence for an arc setting

The central western Junggar area (Fig. 1b) hosts a diverse range of Late Carboniferous (~320 to 310 Ma) and Early Carboniferous (~357 to 330 Ma) basalts. Fig. 5a–b illustrates the variety of settings implied by widely used tectonic discrimination diagrams based on various combinations of relatively immobile elements. The Ti–V diagram (Shervais, 1982) takes advantage of the fact that the multiple valence states and partitioning behavior available to V are sensitive to tectonic settings (e.g., arc magmas are more oxidizing than MORB and within plate basalt (WPB)). Although the Hatu basalts plot in a region of overlap between island arc tholeiites and MORB, the Ti–V diagram

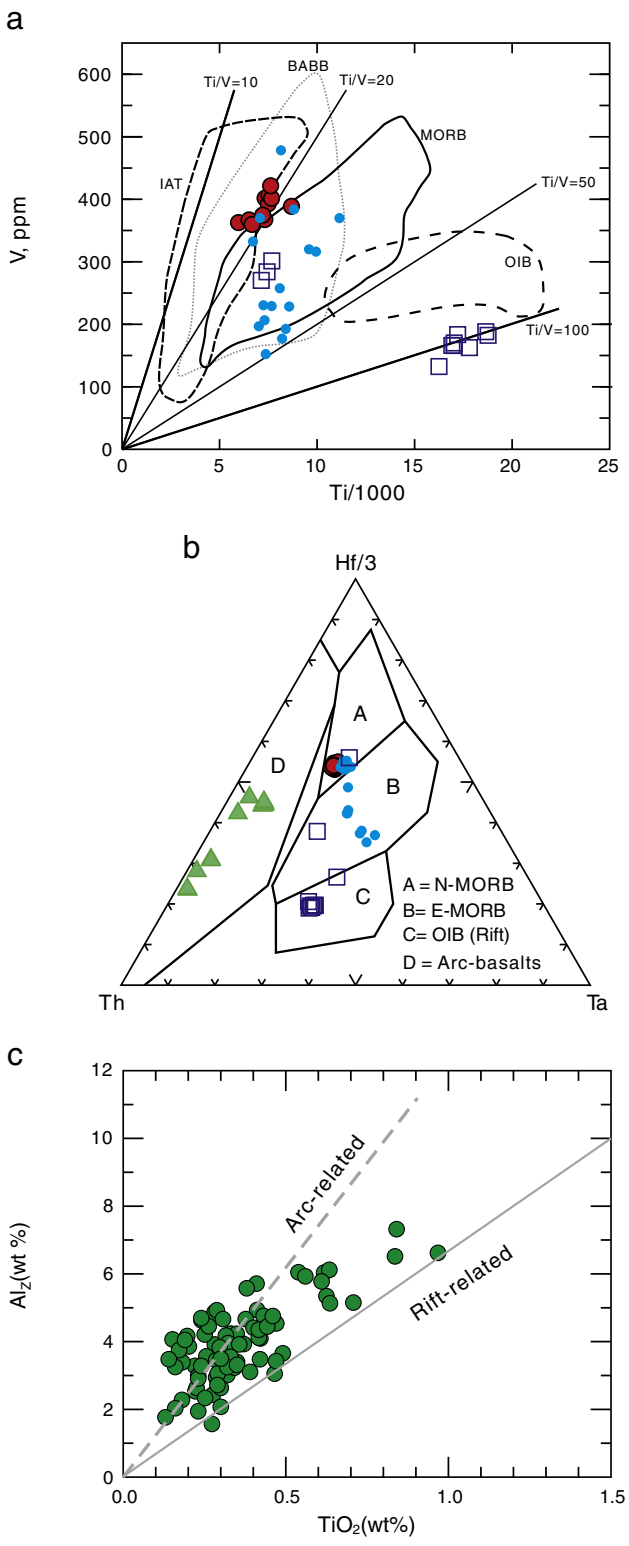

Fig. 5. (a) Ti–V, the fields of MORB, IAT, BABB and OIB are from Shervais (1982), (b) Hf–Th–Ta discrimination diagrams (Wood, 1980). IAT — island arc tholeiite. Data sources and symbols are the same as for Fig. 3. (c) Clinopyroxene chemistry correlations of Al_Z (percentage of tetrahedral sites occupied by Al) versus TiO_2. Reference trends in arc- and rift-related are from Loucks (1990).

demonstrates that the Hatu tholeiites are distinct from most of the Yeyagou and Maliya basalts of the western Junggar area, which mainly plot near the OIB field (Fig. 5a). It is noteworthy, however, that some Yeyagou and Maliya basalts plot in the vicinity of the Hatu basalts, which also fall on a trend defined by the Dalabute ophiolites. The Hf–Th–Ta tectonomagmatic discriminant diagram of Wood (1980) also illustrates that the Hatu basalts overlap with some Yeyagou and Maliya basalts and fall on the Dalabute ophiolite trend. In contrast, the Early Carboniferous basalts plot in the oceanic arc field, showing typical island-arc basalt affinity (Fig. 5b). It is evident that the Early Carboniferous basalts plot along the trend of subduction-zone Th enrichment and differ significantly from the Late Carboniferous basalts. Nonetheless, the Late Carboniferous Hatu, Yeyagou and Maliya basalts are coeval with the 315–310 Ma subducted oceanic crust-derived adakitic rocks in the Baogutu area (western Junggar) (Fig. 1b) that were generated in an arc setting related to ridge subduction and a resultant slab window (Geng et al., 2009; Tang et al., 2010), which is consistent with the arc affinity displayed by the Hatu basalts on Fig. 5a.

The clinopyroxene chemistry provides a further means of establishing the tectonomagmatic affiliation of the Hatu basalts. Basaltic magmas in anorogenic igneous provinces, such as hotspot settings, as a consequence of typically low H_2O and O_2 fugacities relative to arc-axis magmas, are characterized by clinopyroxenes with lower Al_Z/TiO_2 (Al_Z = percentage of tetrahedral sites occupied by Al) (Loucks, 1990). Therefore, on a diagram of Al_Z versus TiO_2 (Fig. 5c), subduction-related clinopyroxenes yield an Al_Z/TiO_2 trend that is roughly twice as steep as that defined by clinoproxenes from rift settings. Most clinopyroxenes from the Hatu basalts plot in the field between the arc- and rift-related compositional trends, showing a deviation from the arc-related trend toward the rift-related trend. Fig. 6a–b shows that, for key chemical discriminators, the Hatu basalts have identical compositional fields to lavas from the Ontong Java and Caribbean oceanic plateau and near primitive mantle values. Given the arc-type signatures of earlier western Junggar basalts and the presence of contemporaneous Baogutu adakites, the results support the interpretation that the Hatu basalts formed in an arc-related extensional setting. Considering both the geological and geochemical features (see detailed discussions in Sections 4.4 and 4.5), the Hatu basalts can best be interpreted as having formed above a slab window related to ridge subduction in an intra-oceanic arc setting.

4.4. Mantle sources and petrogenesis

A "slab window" is formed between the subducted parts of the diverging oceanic plates when a ridge intersects with a subduction zone (Dickinson and Snyder, 1979; Thorkelson, 1996). The "Blowtorch effect" (DeLong et al., 1979) resulting from the upwelling of asthenospheric mantle through the slab window can produce a wide variety of peculiar magmas, ranging from adakites–high-Mg andesites to alkaline and tholeiitic mafic volcanism (Abratis and Worner, 2001; Breitsprecher et al., 2003; Cole and Stewart, 2009; Cole et al., 2006; Gorring et al., 2003; Hastie and Kerr, 2010; Hole et al., 1991; Tang et al., 2010, 2012a,b). Adakites–high-Mg andesites are typically generated by partial melting of subducted slab edge or mafic arc basement. Alkaline and tholeiitic mafic magmas range from depleted MORB to enriched OIB type basalts and are derived from sub-arc lithospheric mantle, sub-slab and/or supra-slab asthenosphere, a subducted lithospheric mantle source, or some mixture of these sources (Cole and Stewart, 2009; Thorkelson et al., 2011). In the following sections, we consider these alternative mantle sources with specific reference to the Hatu tholeiites.

The trace elemental geochemical evidence clearly suggests that the Hatu tholeiites are not derived from supra-slab depleted asthenosphere or sub-arc lithosphere mantle source. The Carboniferous Junggar Ocean, a branch of the Paleo-Asia Ocean, had subducted to the northwest beneath the Keramay arc since the Early Carboniferous

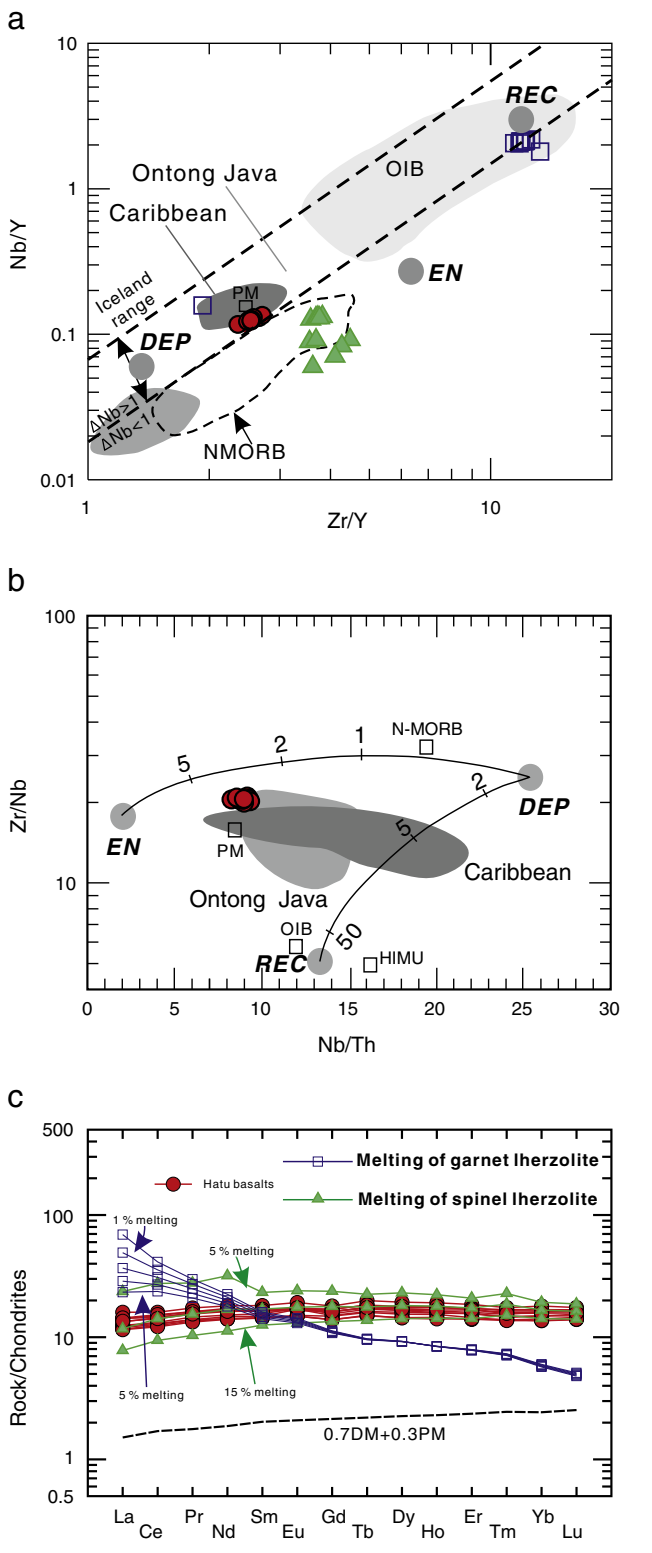

Fig. 6. (a) Nb/Y and Zr/Y variation. The N-MORB and OIB fields, not including Icelandic OIB, are from data compilations of Fitton (2007) and Fitton et al. (1997). The OIB field is data from 780 basalts (MgO > 5 wt.%) from major ocean islands. The N-MORB field is data from the East Pacific Rise, and the Southwest Indian Ridge. (b) Nb/Th and Zr/Nb variation (Condie et al., 2002). Hypothetical mantle end members: DEP, depleted mantle; REC, recycled slab component; EN, enriched mantle components are from Condie (2003). (c) REE modeling results for incongruent dynamic mantle melting for Hatu tholeiitic basalts from the western Junggar. Melting of spinel lherzolite and compared with Hatu tholeiitic basalts. Patterns with symbols are modeling results (patterns are 5% melting increments in melting of spinel lherzolite and 1% increments in garnet lherzolite melting). PM, primitive mantle; DM, depleted MORB mantle. Data sources and symbols are the same as for Fig. 2.

(Tang et al., 2010, 2012a,b). In this scenario, the fluids and/or melts released from the subducted slab would have metasomatised the overlying supra-slab depleted asthenosphere and sub-arc lithosphere mantle sources as observed for the Early Carboniferous basalts and Late Carboniferous mafic-intermediate dikes in the western Junggar region, which show typical "normal" island arc geochemical features reflecting partial melting of the mantle wedge (Geng et al., 2011; Yin et al., 2010). However, the absence of negative Nb, Ta and Ti anomalies on the incompatible element distribution patterns of the Hatu tholeiites indicates that the metasomatised mantle could not have been the source for these basalts.

The Hatu basalts are geochemically similar to the Santa Maria basalts in western California and the Caribou Creek basalts in southern Alaska in having LREE that are slightly enriched compared to N-MORB; both of these basalt suites are considered to have been derived from partial melting of depleted MORB mantle (DMM)-type sub-slab mantle sources (e.g., Cole and Stewart, 2009; Cole et al., 2006). However, the data indicate that this type of depleted mantle was not an important component of the Hatu basalt source. The N-MORB type basalts in pre-Permian ophiolites around the Junggar basin represent the regional DMM isotope composition, which show distinctly higher $\varepsilon_{Nd}(t)$ and lower $^{87}Sr/^{86}Sr(t)$ values than the Hatu basalts (Fig. 4a). The $\varepsilon_{Nd}(t)$ values (+5.25–+5.94) of the Hatu tholeiites are also distinctly lower than those of the slab-derived contemporaneous Baogutu adakites ($\varepsilon_{Nd}(t) = +5.8–+8.3$) (Tang et al., 2010). The Hatu basalts are not as depleted as average N-MORB, as their Zr/Nb ratios are clearly lower than N-MORB (Supplemental file 8). Plots of $\varepsilon_{Nd}(t)$ against Zr/Nb (Supplemental file 8d) clearly distinguish the Hatu samples from the DMM-derived N-MORB-type basalts in pre-Permian ophiolites around the Junggar basin. The initial $^{187}Os/^{188}Os$ values (0.1338 to 0.3457) are considerably higher than the accepted upper limit of global MORB (Shirey and Walker, 1998). The basalts are also enriched in incompatible elements relative to N-MORB, indicating an origin from a more enriched source than DMM. Thus, the balance of evidence suggests that the Hatu tholeiites were not solely derived from a sub-slab DMM-type mantle source in a slab window.

A sub-slab enriched OIB source involving the deep asthenospheric mantle can also be ruled out as a sole source for the Hatu basalts. Magmas generated entirely by partial melting of such a mantle source would have a strong OIB-like geochemical signature. For example, enriched alkaline and tholeiitic OIB-type basalts from the Patagonian Cordillera in South America, Baja California, Mexico, and western Canada, associated with ridge subduction and resultant slab window, all have strong OIB-like geochemical signatures (Gorring et al., 2003; Pallares et al., 2007; Thorkelson et al., 2011). However, the Hatu basalts show predominantly flat Chondrite and N-MORB normalized multi-element patterns, clearly contrasting with OIB-type magmas.

It is important to note that the trace element distributions and isotope geochemical compositions of the Hatu basalts share many features in common with those found in modern and Phanerozoic oceanic plateaux (e.g., the Caribbean and Ontong Java plateaux; Kerr et al., 2002; Hastie and Kerr, 2010; Hastie et al., 2008;). The log–log Nb/Y–Zr/Y plot has proved to be a robust discriminant between basalts derived from DMM source regions and from mantle plumes (oceanic island and plateau basalts) and the Zr/Y and Nb/Y ratios display only small variations with low-pressure crystal fractionation and partial melting processes (Fitton et al., 1997). In Fig. 6a, plume-related lavas plot between two parallel lines, and oceanic plateau basalts also plot between these lines (Kerr et al., 1997), whereas N-MORB and arc lavas plot at lower values (Fitton et al., 1997). All the Hatu basalts plot within the plume-derived field along with Caribbean and Ontong Java plateaux data, which are mafic igneous provinces generally attributed to ascending mantle plumes (Kerr et al., 2002). Although the Hatu basalts are geochemically similar to these oceanic plateau basalts and plot in the plume-derived field in the Nb/Y–Zr/Y plot, there is a lack of supporting evidence for their origin in oceanic plateau. Geologically, the volume of the Hatu basalts in the western Junggar region is estimated at ~500 km^3 based on the area of outcrop and stratigraphic thickness. All known examples of mafic magmatism produced by ridge subduction and slab windows have relatively small volumes, such as slab window basalts in southern Alaska (Cole et al., 2006), Southern Patagonia (Gorring et al., 2003) and the Antarctic Peninsula (Hole et al., 1991). Conversely, oceanic plateaus represent much larger melt volumes, on the order of 10^6 km (Hastie and Kerr, 2010). In the western Junggar region, there is no obvious evidence for a mantle plume or hotspot during the Late Carboniferous, although an Early Permian (~275 Ma) mantle plume has been reported in the Tarim Block with related magmatism extending to the northern Xinjiang region (Zhang et al., 2010; Zhou et al., 2004, 2009). In addition to voluminous and predominantly tholeiitic basalts, oceanic plateau magmatic rocks also commonly include minor picrites or komatiites (Hastie and Kerr, 2010; Hastie et al., 2008). In contrast, no such Late Carboniferous ultramafic rock types have been found in the Western Junggar region.

Isotopic data and flat chondrite-normalized REE patterns (Figs. 3 and 4; Supplemental files 6 and 8) show that the mantle source for the Hatu basalts should be less depleted than DMM. On plots of Nb/Y–Zr/Y and Nb/Th–Zr/Nb (Fig. 6a, b), the Hatu samples have intermediate ratios and fall near the primitive mantle along with oceanic plateau basalts such as the Ontong Java and Caribbean Plateaux. Geodynamic models suggest that as much as 20–30% of the Earth's interior may have escaped differentiation (e.g., Brandenburg et al., 2008) and the Hatu basalts have similar isotopic composition to major flood basalt provinces (e.g. Baffin Island, West Greenland, and Ontong Java plateau lavas) that have been proposed to be derived from primitive, albeit non-chondritic, mantle (Jackson and Carlson, 2011; Jackson et al., 2010). However, the Hatu basalts are not flood basalts related to oceanic plateau as discussed above. Oceanic plateau basalts are generally thought to be derived from a mantle source involving mixing between a depleted mantle plume component and a HIMU (high μ) component with a small contribution of an enriched component (Condie et al., 2002; Fitton, 2007; Fitton et al., 1997) (Fig. 6a, b). The depleted mantle plume component comes from a deep source and is an intrinsic part of the plume itself, which was ultimately derived from recycled subducted oceanic lithosphere (Kempton et al., 2000). HIMU represents a recycled component of more-enriched upper oceanic crust (Hofmann, 1997). The enriched component may have inherited a subduction-related component (e.g., subducted continental sediments) (Condie et al., 2002). Given that the Hatu basalt samples plot in or near the field of oceanic plateau basalts on Nb/Y–Zr/Y and Nb/Th–Zr/Nb diagrams (Fig. 6a, b), their mantle source could also correspond to a mixture of these three mantle end members. For example, trace element melting models for the basalts are consistent with a mantle source region composed of subequal amounts of depleted and recycled end members plus a minor enriched mantle component (Fig. 6b).

Incongruent dynamic melting is a common process in the generation of mantle-derived magmas (e.g., Walter, 1998). In order to illuminate the mantle melting history and source mineralogy for the Hatu tholeiitic basalts, we modeled melting of spinel and garnet lherzolites using the incongruent dynamic melting model devised by Zou and Reid (2001). Olivine and orthopyroxene are produced during the reaction Clinopyroxene (Cpx) + Orthopyroxene (Opx) + Spinel (Sp) = melt + olivine (Ol) for spinel peridotites and Cpx + Garnet (Gt) + Ol = melt + Opx for garnet peridotites, respectively (e.g., Walter, 1998). The modeling employed constant partition coefficients, constant net fractional contribution of a phase to the total melt (Zou and Reid, 2001) and partition coefficients from Salters and Stracke (2004) and Shaw (2000). The dynamic mantle melting results indicate that solutions are non-unique, and many factors such as partition coefficients, degree of melting, melt reaction coefficients and source components all jointly affect the model results. Given, however, that the Hatu

tholeiitic basalts are most likely to require melting of a mixed source dominated by depleted spinel lherzolite (Fig. 6c), the melting model suggests that a high degree of melting of an ~10% LREE-depleted source, and 0.7DM + 0.3PM components best reproduce the variation in the Hatu tholeiitic basalts. REE concentrations for the Hatu tholeiitic basalts are not consistent with low-degree (1–5%) melting of garnet lherzolite alone (Fig. 6c). The aggregate melts would have lower concentrations of HREE relative to the Hatu samples. The fact that $(Gd/Yb)_N \approx 1$ in these samples also argues against garnet as an important residual phase. Therefore, the Hatu tholeiitic basalts must represent shallow melting above the garnet–peridotite stability field (Hirschmann and Stolper, 1996).

In contrast to oceanic plateau basalts, we suggest that the depleted mantle source was directly inherited from subducted oceanic lithosphere and the recycled component originated in upwelling enriched deep asthenosphere, possibly through the slab window. Moreover, such an enriched deep asthenosphere is similar to the source of the Late Carboniferous OIB-type alkaline basalts in the western Junngar (Fig. 3) (Buckman and Aitchison, 2004; Liu et al., 2009; Zhang, 2009). The minor enriched source for the Hatu samples is also manifested by highly radiogenic Os isotope compositions ($^{187}Os/^{188}Os_{315Ma}$ = 0.1338–0.3547). One possible mechanism for generating the high initial $^{187}Os/^{188}Os$ is greater degrees of shallow-level crustal assimilation, given that crustal materials generally possess highly radiogenic $^{187}Os/^{188}Os$ compositions (Shirey and Walker, 1998). For the Hatu basalts in an intra-oceanic arc setting (e.g., Geng et al., 2009; Tang et al., 2010, 2012a,b), the arc was most likely composed mainly of young oceanic crust that was too young to possess high $^{187}Os/^{188}Os$ compositions and had low Os concentrations (MORBs with $^{187}Os/^{188}Os$ ratio higher than 0.14 have average Os contents of 3.5 ± 2.4 pg/g) (Escrig et al., 2005). Thus, contamination by such arc crust could not have produced the high initial $^{187}Os/^{188}Os$ and high Os contents (>80 pg/g) of the Hatu basalts, although samples with low Os contents (<60 pg/g) and high initial $^{187}Os/^{188}Os$ ratios may have been slightly modified by shallow level contamination. Another commonly cited mechanism for producing high initial Os isotope ratios in arc lavas is subducted slab input (Alves et al., 2002; Borg et al., 2000; Suzuki and Tatsumi, 2006). However, the lack of subduction-related lithophile element characteristics suggests that subducted materials could not account for the radiogenic $^{187}Os/^{188}Os$ ratios in the Hatu samples. The radiogenic $^{187}Os/^{188}Os$ ratios measured in OIB, particularly in the HIMU islands, likely correspond to recycled subducted oceanic crust with or without sediment in their mantle source regions (Dale et al., 2007; Hauri and Hart, 1993; Reisberg et al., 1993) and were probably also required in the Hatu basalt source to account for their highly radiogenic $^{187}Os/^{188}Os$ compositions and enriched source.

4.5. Slab window asthenosphere–lithosphere interaction during ridge subduction

Massive Phanerozoic granitoids with notably positive $\varepsilon_{Nd}(t)$ values are widely distributed in the CAOB, and are regarded as products of extensive basalts underplating in a post-orogenic or an intraplate extensional setting (Jahn et al., 2000; Wu et al., 2002). Conversely, Windley et al. (2007) suggested that the CAOB contains many key features (e.g., adakites, boninites, near-trench magmatism, Alaskan-type mafic–ultramafic complexes and high-temperature metamorphic belts) that are explicable by ridge–trench interactions, and claimed that there could have been at least seven ridge subduction events during the evolution of the CAOB (1000 Ma–250 Ma). Recent studies support the occurrence of ridge subduction in the CAOB, based on the association of ophiolites, adakites, high Mg andesitic rocks, and A-type granites (Geng et al., 2009; Jian et al., 2008; Tang et al., 2010, 2012a,b; Yin et al., 2010) and zircon U–Pb and Hf isotopic studies (Sun et al., 2009). In this model, granitoids with positive $\varepsilon_{Nd}(t)$ values are produced above a slab window resulting from ridge subduction. In the western Junggar region, the petrogenesis and tectonic environments of the Late Carboniferous to Early Permian granitoids (320–290 Ma) are controversial, with two main competing viewpoints, i.e., post-collisional (Chen and Arakawa, 2005; Han et al., 2006; Su et al., 2006) versus an island arc environment related to intra-oceanic subduction or ridge subduction (Geng et al., 2009; Tang et al., 2010, 2012a,b; Xiao et al., 2008; Yin et al., 2010; Zhang et al., 2006). Our recent study demonstrates that the Late Carboniferous Baogutu adakites (315–310 Ma), located in the central area of the western Junggar region, are typical of arc magmatism generated by partial melting of a slab edge close to a subducting spreading ridge (Tang et al., 2010).

Tectonic and petrogenetic models for the Late Carboniferous basalts need to account for: (1) the occurrence of Late Carboniferous contemporaneous oceanic plateau like tholeiites (Hatu) and OIB like alkaline basalts (Yeyagou–Maliya) in an intra-oceanic arc setting, coeval with slab-derived adakites; (2) the variety of mantle source regions for the Late Carboniferous basalts; (3) minimal crustal assimilation; (4) the appearance of voluminous slightly younger A-type granitic

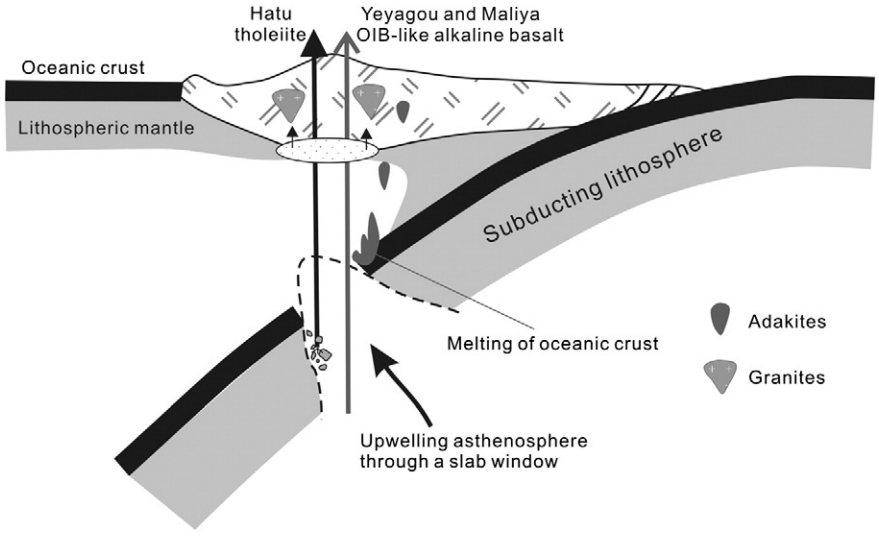

Fig. 7. Conceptual diagram illustrating the tectonic and magmatic rocks evolution of the western Junggar during Late Carboniferous to Early Permian (~320–290 Ma). A slab window formed in response to a spreading ridge subduction beneath the Keramay arc, forming different types of basalts.

rocks (310–290 Ma) with positive and high $\varepsilon_{Nd}(t)$ values; and (5) the numerous Late Carboniferous Cu–Au deposits that occur in the western Junggar region. We propose that heterogeneous mantle associated with spreading ridge subduction and a slab window along the southeastern margin of the western Junggar region, coupled with regional crustal extension, can account for these features (Fig. 7). In fact, mafic rocks produced in response to decompression melting of mantle upwelling through a slab window commonly display geochemical characteristics ranging from depleted MORB-like mantle (e.g., southern Alaska) to enriched OIB-like mantle (e.g., southern Patagonia) (Cole and Stewart, 2009; Cole et al., 2006; D'Orazio et al., 2001; Gorring et al., 2003; Hole et al., 1991). Accordingly, these mafic rocks are likely to be straightforward manifestations of the spreading ridge subduction–slab window environment.

The Hatu basalts offer an opportunity to decipher the mantle sources of tholeiitic magmas through the application of the ridge subduction and slab window model. We propose that the crust of the Junggar Ocean (one branch of the Paleo-Asia Ocean) subducted to the northwestward (in present coordinates) at ~350–330 Ma and formed the Keramay intra-oceanic arc. During this process, upwelling slab-derived fluids would have triggered partial melting of the mantle wedge, forming volcanic rocks with typical "island arc-type" geochemical compositions ranging from basalts to felsic rocks (Geng et al., 2011; Tang et al., 2010, 2012a,b). These magmatic rocks are the main components of the Keramay intra-oceanic arc. Previous studies mainly focused on the felsic rocks, such as adakites and I- and A-type granites (Geng et al., 2011; Tang et al., 2010, 2012a,b). However, in a slab window setting, sub- and supra-slab mantle reservoirs and the down-going slab itself may all act as sources for basaltic magmas, producing basalts with depleted MORB-like to enriched OIB-like compositions (e.g., Thorkelson et al., 2011). Therefore, the presence of MORB-type basalts coeval with the adakites and I- and A-type granites provide strong additional evidence for Late Carboniferous ridge subduction in the western Junggar district (Fig. 7).

The Hatu tholeiites can be interpreted as the product of mantle sources created by the infiltration of decompression melts (from upwelling enriched asthenosphere) into the subducted lithosphere (Fig. 7). The infiltrating melts reacted with peridotites to form the metasomatized mantle source and the Hatu tholeiites were likely generated by large degrees of partial melting of this mantle source at shallow depths. In contrast, the more isotopically enriched Yeyagou and Maliya alkaline basalts are consistent with an enriched mantle source similar to that of OIB (Zhang, 2009) and are most plausibly derived from small-degree melts at greater depths, without the involvement of depleted subducted oceanic lithospheric mantle.

Ridge subduction and resultant slab windows may also be responsible for the formation of the intermediate-acid rocks (adakitic rocks, I-type granitoids and A-type granite) in the western Junggar region (Geng et al., 2009; Shen et al., 2009; Tang et al., 2010, 2012a,b; Zhang et al., 2006). Thorkelson and Breitsprecher (2005) identified slab windows in particular as important sites for slab melting, suggesting that the thin lithosphere around the edges of slab windows are most likely to thermally equilibrate and partially melt. The Baogutu adakitic rocks were most likely generated by partial melting of a slab edge close to a subducting spreading ridge in the garnet amphibolite faces as a result of a ridge subduction (Tang et al., 2010). Similar events generated Costa Rican adakitic rocks above the Cocos-Nazca slab window beneath Central America (Johnston and Thorkelson, 1997). Partial melting of the juvenile lower crust, triggered by upwelling asthenosphere and basaltic underplating through a slab window, could also promote the formation of I- and A-type granites (Fig. 7). Finally, ridge subduction and the resulting slab window also have a genetic link to the western Junggar Cu–Au deposits, given the documented links between gold deposits and slab windows in southern Alaska and other parts of the Pacific margin (Goldfarb et al., 1998; Haeussler et al., 1995).

5. Conclusions

The Hatu tholeiites in the western Junggar region erupted at ~315 Ma, and were derived from a mixed mantle source consisting of subducted depleted oceanic lithosphere and deep, enriched upwelling asthenospheric mantle. These requirements are most consistent with generation of Late Carboniferous tholeiites in the western Junggar area in a ridge subduction and resultant slab window model. The Hatu tholeiites were generated by interaction of asthenospheric melts with eroded oceanic lithospheric mantle, caused by upwelling asthenosphere through the slab window. Ridge subduction and associated slab window formation were also responsible for the formation of the regional intermediate-acid rocks and Cu–Au deposits, and probably played an important role in Paleozoic crustal growth of CAOB.

Acknowledgments

We sincerely appreciate the detailed and constructive reviews and suggestions of Professor Rick Carlson and two anonymous reviewers, which greatly improved this paper. We also appreciate the assistance of Jinhui Yang, Jifeng Xu, Guiqing Wang, Yueheng Yang, Liewei Xie, Ying Liu, Guangqian Hu, Jinlong Ma, Xirong Liang and Xianglin Tu for geochemical analyses. This study was jointly supported by the Major State Basic Research Program (973 Program) of the People's Republic of China (nos. 2010CB808906 and 2007CB411308), and the National Natural Science Foundation of China (grant nos. 41025006, 41073029 and 41121002). This is contribution no. IS-1462 from GIGCAS, and contribution 34 from the ARC Centre of Excellence for Core to Crust Fluid Systems (http://www.ccfs.mq.edu.au).

Appendix A. Supplementary data

Supplementary data to this article can be found online at doi:10.1016/j.epsl.2012.02.009.

References

Abratis, M., Worner, G., 2001. Ridge collision, slab-window formation, and the flux of Pacific asthenosphere into the Caribbean realm. Geology 29, 127–130.
Alves, S., Schiano, P., Capmas, F., Allègre, C.J., 2002. Osmium isotope binary mixing arrays in arc volcanism. Earth Planet. Sci. Lett. 198, 355–369.
An, F., Zhu, Y.F., 2009. SHRIMP U–Pb zircon ages of the tuff in Baogutu Formation and their geological significances. Acta Petrol. Sin. 25, 1437–1445 (in Chinese with English abstract).
Beijing SHRIMP Unit, 2005. Annual Report of Beijing SHRIMP Unit. Geological Press, Beijing, pp. 1–71.
Blichert-Toft, J., Albarède, F., 1997. The Lu–Hf isotope geochemistry of chondrites and the evolution of the mantle–crust system. Earth Planet. Sci. Lett. 148, 243–258.
Borg, L.E., Brandon, A.D., Clynne, M.A., Walker, R.J., 2000. Re–Os isotopic systematics of primitive lavas from the Lassen region of the Cascade arc, California. Earth Planet. Sci. Lett. 177, 301–317.
Brandenburg, J.P., Hauri, E.H., van Keken, P.E., Ballentine, C.J., 2008. A multiple-system study of the geochemical evolution of the mantle with force-balanced plates and thermochemical effects. Earth Planet. Sci. Lett. 276, 1–13.
Breitsprecher, K., Thorkelson, D.J., Groome, W.G., Dostal, J., 2003. Geochemical confirmation of the Kula–Farallon slab window beneath the Pacific Northwest in Eocene time. Geology 31, 351–354.
Buckman, S., Aitchison, J.C., 2004. Tectonic evolution of Palaeozoic terranes in West Junggar, Xinjiang, NW China. In: Malpas, J., Fletcher, C.J., Aitchison, J.C., Ali, J. (Eds.), Aspects of the Tectonic Evolution of China. Geological Society, London, Special Publications, pp. 101–129.
Chauvel, C., Lewin, E., Carpentier, M., Arndt, N.T., Marini, J.C., 2008. Role of recycled oceanic basalt and sediment in generating the Hf–Nd mantle array. Nat. Geosci. 1, 64–67.
Chen, B., Arakawa, Y., 2005. Elemental and Nd–Sr isotopic geochemistry of granitoids from the West Junggar foldbelt (NW China), with implications for Phanerozoic continental growth. Geochim. Cosmochim. Acta 69, 1307–1320.
Cole, R.B., Stewart, B.W., 2009. Continental margin volcanism at sites of spreading ridge subduction: examples from southern Alaska and western California. Tectonophysics 464, 118–136.
Cole, R.B., Nelson, S.W., Layer, P.W., Oswald, P.J., 2006. Eocene volcanism above a depleted mantle slab window in southern Alaska. Geol. Soc. Am. Bull. 118, 140–158.

Condie, K.C., 2003. Incompatible element ratios in oceanic basalts and komatiites: tracking deep mantle sources and continental growth rates with time. Geochem. Geophys. Geosyst. 4, 1005. doi:10.1029/2002GC000333.
Condie, K.C., Frey, B.A., Kerrich, R., 2002. The 1.75-Ga Iron King Volcanics in west-central Arizona: a remnant of an accreted oceanic plateau derived from a mantle plume with a deep depleted component. Lithos 64, 49–62.
Constantin, M., 1999. Gabbroic intrusions and magmatic metasomatism in harzburgites from the Garrett transform fault: implications for the nature of the mantle–crust transition at fast-spreading ridges. Contrib. Mineral. Petrol. 136, 111–130.
Dale, C.W., Gannoun, A., Burton, K.W., Argles, T.W., Parkinson, I.J., 2007. Rhenium–osmium isotope and elemental behaviour during subduction of oceanic crust and the implications for mantle recycling. Earth Planet. Sci. Lett. 253, 211–225.
DeLong, S.E., Schwarz, W.M., Anderson, R.N., 1979. Thermal effects of ridge subduction. Earth Planet. Sci. Lett. 44, 239–246.
Dickinson, W.R., Snyder, W.S., 1979. Geometry of subducted slabs related to San Andreas transform. J. Geol. 87, 609–627.
D'Orazio, M., Agostini, S., Innocenti, F., Haller, M.J., Manetti, P., Mazzarini, F., 2001. Slab window-related magmatism from southernmost South America: the Late Miocene mafic volcanics from the Estancia Glencross Area (52°S, Argentina–Chile). Lithos 57, 67–89.
Escrig, S., Schiano, P., Schilling, J.G., Allègre, C.J., 2005. Rhenium–Osmium isotope Systematics in MORB from the Southern Mid-Atlantic Ridge (40°–50°S). Earth Planet. Sci. Lett. 235, 528–548.
Fitton, J.G., 2007. The OIB paradox. Geol. Soc. Am. Spec. Pap. 430, 387–412.
Fitton, J.G., Godard, M., 2004. Origin and evolution of magmas on the Ontong Java Plateau. Geol. Soc. Lond. Spec. Publ. 229, 151–178.
Fitton, J.G., Saunders, A.D., Norry, M.J., Hardarson, B.S., Taylor, R.N., 1997. Thermal and chemical structure of the Iceland plume. Earth Planet. Sci. Lett. 153, 197–208.
Fretzdorff, S., Schwarz-Schampera, U., Gibson, H.L., Garbe-Schöberg, C.D., Hauff, F., Stoffers, P., 2006. Hydrothermal activity and magma genesis along a propagating back-arc basin: Valu Fa Ridge (southern Lau Basin). J. Geophys. Res. 111, B08205.
Geng, H., Sun, M., Yuan, C., Xiao, W., Xian, W., Zhao, G., Zhang, L., Wong, K., Wu, F., 2009. Geochemical, Sr–Nd and zircon U–Pb–Hf isotopic studies of Late Carboniferous magmatism in the West Junggar, Xinjiang: implications for ridge subduction? Chem. Geol. 266, 364–389.
Geng, H.Y., Sun, M., Yunan, C., Zhao, G.C., Xiao, W.J., 2011. Geochemical and geochronological study of early Carboniferous volcanic rocks from the West Junggar: petrogeneses and tectonic implications. J. Asian Earth. Sci. 42, 854–866.
Goldfarb, R.J., Phillips, G.N., Nokleberg, W.J., 1998. Tectonic setting of synorogenic gold deposits of the Pacific Rim. Ore. Geol. Rev. 13, 185–218.
Gorring, M., Singer, B., Gowers, J., Kay, S.M., 2003. Plio-Pleistocene basalts from the Meseta del Lago Buenos Aires, Argentina: evidence for asthenosphere–lithosphere interactions during slab window magmatism. Chem. Geol. 193, 215–235.
Haeussler, P.J., Bradley, D.C., Goldfarb, R.J., Snee, L.W., Taylor, C.D., 1995. Link between ridge subduction and gold mineralization in Southern Alaska. Geology 23, 995–998.
Han, B.F., Ji, J.Q., Song, B., Chen, L.H., Zhang, L., 2006. Late Paleozoic vertical growth of continental crust around the Junggar Basin, Xinjiang, China (Part I): timing of post-collisional plutonism. Acta Petrol. Sin. 22, 1077–1086 (in Chinese with English abstract).
Hastie, A.R., Kerr, A.C., 2010. Mantle plume or slab window? Physical and geochemical constraints on the origin of the Caribbean oceanic plateau. Earth Sci. Rev. 98, 283–293.
Hastie, A.R., Kerr, A.C., Mitchell, S.F., Millar, I.L., 2008. Geochemistry and petrogenesis of Cretaceous oceanic plateau lavas in eastern Jamaica. Lithos 101, 323–343.
Hauri, E.H., Hart, S.R., 1993. ReOs isotope systematics of HIMU and EMII oceanic island basalts from the south Pacific Ocean. Earth Planet. Sci. Lett. 114, 353–371.
Hirschmann, M.M., Stolper, E.M., 1996. A possible role for garnet pyroxenite in the origin of the "garnet signature" in MORB. Contrib. Mineral. Petrol. 124, 185–208.
Hofmann, A.W., 1997. Mantle geochemistry: the message from oceanic volcanism. Nature 385, 219–229.
Hole, M.J., Rogers, G., Saunders, A.D., Storey, M., 1991. Relation between alkalic volcanism and slab-window formation. Geology 19, 657–660.
Hu, A.Q., Wang, Z.G., Tu, G.Z., 1997. Geological Evolution and Diagenic and Metallogenetic Regularity in Northern Xinjiang. Science Press, Beijing. (in Chinese with English abstract).
Jackson, M.G., Carlson, R.W., 2011. An ancient recipe for flood-basalt genesis. Nature 476, 316–319.
Jackson, M.G., Carlson, R.W., Kurz, M.D., Kempton, P.D., Francis, D., Blusztajn, J., 2010. Evidence for the survival of the oldest terrestrial mantle reservoir. Nature 466, 853–856.
Jahn, B.M., Wu, F.Y., Chen, B., 2000. Massive granitoid generation in Central Asia: Nd isotope evidence and implication for continental growth in the Phanerozoic. Episodes 23, 82–92.
Jian, P., Liu, D.Y., Kroner, A., Windley, B.F., Shi, Y., Zhang, F., Shi, G., Miao, L., Zhang, W., Zhang, Q., Zhang, L., Ren, J., 2008. Time scale of an early to mid-Paleozoic orogenic cycle of the long-lived Central Asian Orogenic Belt, Inner Mongolia of China: implications for continental growth. Lithos 101, 233–259.
Johnson, K.T.M., Dick, H.J.B., Shimizu, N., 1990. Melting in the oceanic upper mantle: an ion microprobe study of diopsides in abyssal peridotites. J. Geophys. Res. 95, 2661–2678.
Johnston, S.T., Thorkelson, D.J., 1997. Cocos–Nazca slab window beneath Central America. Earth Planet. Sci. Lett. 146, 465–474.
Kempton, P.D., Fitton, J.G., Saunders, A.D., Nowell, G.M., Taylor, R.N., Hardarson, B.S., Pearson, G., 2000. The Iceland plume in space and time: a Sr–Nd–Pb–Hf study of the North Atlantic rifted margin. Earth Planet. Sci. Lett. 177, 255–271.
Kerr, A.C., Marriner, G.F., Tarney, J., Nivia, A., Saunders, A.D., Thirlwall, M.F., Sinton, C.W., 1997. Cretaceous Basaltic Terranes in western Columbia: elemental, chronological and Sr–Nd isotopic constraints on petrogenesis. J. Petrol. 38, 677–702.
Kerr, A.C., Tarney, J., Kempton, P.D., Spadea, P., Nivia, A., Marriner, G.F., Duncan, R.A., 2002. Pervasive mantle plume head heterogeneity: evidence from the late Cretaceous Caribbean–Colombian oceanic plateau. J. Geophys. Res. 107, 2140.
Kröner, A., Windley, B.F., Badarch, G., Tomurtogoo, O., Hegner, E., Jahn, B.M., Gruschka, S., Khain, E.V., Demoux, A., Wingate, M.T.D., 2007. Accretionary growth and crust formation in the Central Asian Orogenic Belt and comparison with the Arabian–Nubian shield. Geol. Soc. Am. Mem. 200, 181–209.
Li, H.Q., Chen, F.W., Cai, H., 2000. Study on Rb–Sr isotopic ages of gold deposits in West Junggar Area, Xinjiang. Acta Geol. Sin. 74, 181–192.
Liu, X.J., Xu, J.F., Wang, S.Q., Hou, Q.Y., Bai, Z.H., Lei, M., 2009. Geochemistry and dating of E-MORB type mafic rocks from Dalabute ophiolite in West Junggar, Xinjiang and geological implications. Acta Petrol. Sin. 25, 1373–1389 (in Chinese with English abstract).
Loucks, R.R., 1990. Discrimination of ophiolitic from nonophiolitic ultramafic–mafic allochthons in orogenic belts by the Al/Ti ratio in clinopyroxene. Geology 18, 346–349.
Miyashiro, A., 1974. Volcanic rock series in island arcs and active continental margins. Am. J. Sci. 274, 321–355.
Pallares, C., Maury, R.C., Bellon, H., Royer, J.-Y., Calmus, T., Aguillón-Robles, A., Cotten, J., Benoit, M., Michaud, F., Bourgois, J., 2007. Slab-tearing following ridge–trench collision: evidence from Miocene volcanism in Baja California, MÈxico. J. Volcanol. Geotherm. Res. 161, 95–117.
Pearce, J.A., Stern, R.J., Bloomer, S.H., Fryer, P., 2005. Geochemical mapping of the Mariana arc-basin system: implications for the nature and distribution of subduction components. Geochem. Geophys. Geosyst. 6, Q07006. doi:10.1029/2004GC000895.
Polat, A., Hofmann, A.W., 2003. Alteration and geochemical patterns in the 3.7–3.8 Ga Isua greenstone belt, West Greenland. Precambrian Res. 126, 197–218.
Polat, A., Hofmann, A.W., Rosing, M.T., 2002. Boninite-like volcanic rocks in the 3.7–3.8 Ga Isua greenstone belt, West Greenland: geochemical evidence for intra-oceanic subduction zone processes in the early Earth. Chem. Geol. 184, 231–254.
Reisberg, L., Zindler, A., Marcantonio, F., White, W., Wyman, D., Weaver, B., 1993. Os isotope systematics in ocean island basalts. Earth Planet. Sci. Lett. 120, 149–167.
Salters, V.J.M., Stracke, A., 2004. Composition of the depleted mantle. Geochem. Geophys. Geosyst. 5, Q05B07. doi:10.1029/2003GC000597.
Sengör, A.M.C., Natal'in, B.A., 1996. Turkic-type orogeny and its role in the making of the continental crust. Annu. Rev. Earth Planet. Sci. 24, 263–337.
Sengör, A.M.C., Natal'in, B.A., Burtman, V.S., 1993. Evolution of the Altaid tectonic collage and Palaeozoic crustal growth in Eurasia. Nature 364, 299–307.
Shaw, D.M., 2000. Continuous (dynamic) melting theory revisited. Can. Mineral. 38, 1041–1063.
Shen, Y.C., Jin, C.W., Zhang, X.Q., 1993. The relationships of magma activity and tectonic setting with gold mineralization in west Junggar. In: Tu, G.Z. (Ed.), New Improvement of Solid Geosciences in Northern Xinjiang. Science Press, Beijing, pp. 137–150.
Shen, P., Shen, Y., Liu, T., Meng, L., Dai, H., Yang, Y., 2009. Geochemical signature of porphyries in the Baogutu porphyry copper belt, western Junggar, NW China. Gondwana Res. 16, 227–242.
Shen, P., Shen, Y., Pan, H., Li, X., Wang, J., Zhu, H., Dai, H., Guan, W., 2012. Geochronology and isotope geochemistry of the Baogutu porphyry copper deposit in the West Junggar Region, Xinjiang, China. J. Asian Earth Sci. doi:10.1016/j.jseaes.2011.1011.1025.
Shervais, J.W., 1982. Ti–V plots and the petrogenesis of modern and ophiolitic lavas. Earth Planet. Sci. Lett. 59, 101–118.
Shinjo, R., Chung, S.-L., Kato, Y., Kimura, M., 1999. Geochemical and Sr–Nd isotopic characteristics of volcanic rocks from the Okinawa Trough and Ryukyu Arc: implications for the evolution of a young, intracontinental back arc basin. J. Geophys. Res. 104, 10591–10608.
Shirey, S.B., Walker, R.J., 1998. The Re–Os isotope system in cosmochemistry and high-temperature geochemistry. Annu. Rev. Earth Plant Sci. 26, 423–500.
Song, H.X., Liu, Y.L., Qu, W.J., Song, B., Zhang, R., Cheng, Y., 2007. Geological characters of Baogutu porphyry copper deposit in Xinjiang, NW China. Acta Petrol. Sin. 23, 1981–1988 (in Chinese with English abstract).
Su, Y.P., Tang, H.F., Hong, G.S., Liu, C.Q., 2006. Geochemistry of aluminous A-type granites along Darabut tectonic belt in West Junggar, Xinjiang. Geochima 35, 55–67 (in Chinese with English abstract).
Sun, S.S., McDonough, W.F., 1989. Chemical and isotopic systematics of oceanic basalts: implications for mantle composition and processes. In: Saunders, A.D., Norry, M.J. (Eds.), Magmatism in the Ocean Basins: Geological Society London Special Publications, vol. 42, pp. 313–345.
Sun, M., Long, X.P., Cai, K.D., Jiang, Y.D., B.Y, W., Yuan, C., Zhao, G.C., Xiao, W.J., Wu, F.Y., 2009. Early Paleozoic ridge subduction in the Chinese Altai: insight from the abrupt change in zircon Hf isotopic compositions. Sci. China Ser. D 39, 1–14.
Suzuki, K., Tatsumi, Y., 2006. Re–Os systematics of high-Mg andesites and basalts from the Setouchi volcanic belt, SW Japan: implications for interaction between wedge mantle and slab-derived melt. Geochem. J. 40, 297–307.
Tang, G.-J., Wang, Q., Wyman, D.A., Li, Z.-X., Zhao, Z.-H., Jia, X.-H., Jiang, Z.-Q., 2010. Ridge subduction and crustal growth in the Central Asian Orogenic Belt: Evidence from Late Carboniferous adakites and high-Mg diorites in the western Junggar region, northern Xinjiang (west China). Chem. Geol. 227, 281–300.
Tang, G.-J., Wang, Q., Wyman, D.A., Li, Z.X., Xu, Y.G., Zhao, Z.H., 2012a. Recycling oceanic crust for continental crustal growth: Sr–Nd–Hf isotope evidence from granotoids in the western Junggar region, NW China. Lithos 128–131, 73–83.
Tang, G.-J., Wang, Q., Wyman, D.A., Li, Z.-X., Zhao, Z.-H., Yang, Y.-H., 2012b. Late Carboniferous high $\varepsilon Nd(t)$–$\varepsilon Hf(t)$ granitoids, enclaves and dikes in western Junggar, NW China: ridge-subduction-related magmatism and crustal growth. Lithos 140–141, 85–101.

Thorkelson, D.J., 1996. Subduction of diverging plates and the principles of slab window formation. Tectonophysics 255, 47–63.
Thorkelson, D.J., Breitsprecher, K., 2005. Partial melting of slab window margins: genesis of adakitic and non-adakitic magmas. Lithos 79, 25–41.
Thorkelson, D.J., Madsen, J.K., Sluggett, C.L., 2011. Mantle flow through the Northern Cordilleran slab window revealed by volcanic geochemistry. Geology 39, 267–270.
Vervoort, J.D., Patchett, P.J., Blichert-Toft, J., Albarede, F., 1999. Relationships between Lu-Hf and Sm-Nd isotopic systems in the global sedimentary system. Earth Planet. Sci. Lett. 168, 79–99.
Walter, M.J., 1998. Melting of garnet peridotite and the origin of komatiite and depleted lithosphere. J. Petrol. 39, 29–60.
Wang, R., Zhu, Y.F., 2007. Geology of the Baobei gold deposit in western Juggar and zircon SHRIMP age of its wall-rocks, western Junggar (Xinjiang, NW China). Geol. J. China Univ. 13, 590–602.
Wilson, M., 1989. Igneous Petrogenesis. Springer, Harper Collins Academic, London.
Winchester, J.A., Floyd, P.A., 1977. Geochemical discrimination of different magma series and their differentiation products using immobile elements. Chem. Geol. 20, 325–343.
Windley, B.F., Alexeiev, D., Xiao, W., Kroner, A., Badarch, G., 2007. Tectonic models for accretion of the Central Asian Orogenic Belt. J. Geol. Soc. Lond. 164, 31–47.
Wood, D.A., 1980. The application of a Th–Hf–Ta diagram to problems of tectonomagmatic classification and to establishing the nature of crustal contamination of basaltic lavas of the British Tertiary Volcanic Province. Earth Planet. Sci. Lett. 50, 11–30.
Wu, F.Y., Sun, D.Y., Li, H.M., Jahn, B.M., Wilde, S., 2002. A-type granites in northeastern China: age and geochemical constraints on their petrogenesis. Chem. Geol. 187, 143–173.
Xiao, W.J., Han, C.M., Yuan, C., Sun, M., Lin, S.F., Chen, H.L., Li, Z.L., Li, J.L., Sun, S., 2008. Middle Cambrian to Permian subduction-related accretionary orogenesis of Northern Xinjiang, NW China: implications for the tectonic evolution of central Asia. J. Asian Earth Sci. 32, 102–117.
Xu, J.-F., Castillo, P.R., Chen, F.-R., Niu, H.-C., Yu, X.-Y., Zhen, Z.-P., 2003. Geochemistry of late Paleozoic mafic igneous rocks from the Kuerti area, Xinjiang, northwest China: implications for backarc mantle evolution. Chem. Geol. 193, 137–154.
Xu, Y.-G., Ma, J.-L., Frey, F.A., Feigenson, M.D., Liu, J.-F., 2005. Role of lithosphere–asthenosphere interaction in the genesis of Quaternary alkali and tholeiitic basalts from Datong, western North China Craton. Chem. Geol. 224, 247–271.
Xu, X., He, G.Q., Li, H.Q., Ding, T.F., Liu, X.Y., Mei, S.W., 2006a. Basic characteristics of the Karamay ophiolitic mélange, Xinjiang, and its zircon SHRIMP dating. Geol. China 33, 470–475 (in Chinese with English abstract).
Xu, X.Y., Xia, L.Q., Ma, Z.P., Wang, Y.B., Xia, Z.C., Li, X.M., Wang, L.S., 2006b. SHRIMP zircon U–Pb geochronology of the plagiogranites from Bayringou ophiolite in North Tianshan Mountains and the petrogenesis of the ophiolite. Acta Petrol. Sin. 22, 83–94 (in Chinese with English abstract).
Yin, J., Yuan, C., Sun, M., Long, X., Zhao, G., Wong, K.P., Geng, H., Cai, K., 2010. Late Carboniferous high-Mg dioritic dikes in Western Junggar, NW China: geochemical features, petrogenesis and tectonic implications. Gondwana Res. 17, 145–152.
Zhang, J.N., 2009. Late Paleozoic Accretionary Tectonics of the Eastern Part of Western Junggar, Xinjiang: Insights from Anatomy of the Ophiolitic Mélange and Accretionary Complex. Institute of Geology and Geophysics, Chinese Academy of Sciences, Beijing, p. 195.
Zhang, L.C., Wan, B., Jiao, X.J., Zhang, R., 2006. Characteristics and geological significance of adakitic rocks in copper-bearing porphyry in Baogutu, western Junggar. Geol. China 33, 626–631 (in Chinese with English abstract).
Zhang, C.L., Li, Z.X., Li, X.H., Xu, Y.G., Zhou, G., Ye, H.M., 2010. A Permian large igneous province in Tarim and Central Asian Orogenic Belt (CAOB), NW China: results of a ca. 275 Ma mantle plume? Geol. Soc. Am. Bull. 122, 2020–2040.
Zhou, M.F., Michael Lesher, C., Yang, Z.G., Li, J.W., Sun, M., 2004. Geochemistry and petrogenesis of 270 Ma Ni–Cu–(PGE) sulfide-bearing mafic intrusions in the Huangshan district, Eastern Xinjiang, Northwest China: implications for the tectonic evolution of the Central Asian orogenic belt. Chem. Geol. 209, 233–257.
Zhou, M.-F., Zhao, J.-H., Jiang, C.-Y., Gao, J.-F., Wang, W., Yang, S.-H., 2009. OIB-like, heterogeneous mantle sources of Permian basaltic magmatism in the western Tarim Basin, NW China: implications for a possible Permian large igneous province. Lithos 113, 583–594.
Zou, H., Reid, M.R., 2001. Quantitative modeling of trace element fractionation during incongruent dynamic melting. Geochim. Cosmochim. Acta 65, 153–162.